

# Supporting Information

## Low temperature dry reforming of methane over Pt/CeO<sub>2</sub>, Ni/CeO<sub>2</sub> and Pt-Ni/CeO<sub>2</sub> catalysts prepared by solution-combustion method

Rubina Khatun,<sup>a,b</sup> Nazia Siddiqui,<sup>a,b</sup> Rohan Singh Pal,<sup>a,b</sup> Sonu Bhandari,<sup>a,b</sup> Tuhin Suvra Khan,<sup>a,b</sup> Shivani Singh,<sup>a</sup> Mukesh Kumar Poddar,<sup>a</sup> Chanchal Samanta,<sup>c</sup> and Rajaram Bal,<sup>\*a,b</sup>

<sup>a</sup>Light Stock Processing Division, CSIR-Indian Institute of Petroleum, Dehradun 248005, India. Fax: +91 135 2660202; Tel: +91 135 2525917.

<sup>b</sup>Academy of Scientific and Innovative Research (AcSIR), Ghaziabad- 201002, India.

<sup>c</sup>Bharat Petroleum Corporation Ltd., Greater Noida, Uttar Pradesh, 201306, India

\*Corresponding author: raja@iip.res.in; Fax: +91 135 2660202; Tel: +91 135 2525917

### S1 Experimental:

#### S1.1 Materials

Tetraamineplatinum nitrate [Pt(NH<sub>3</sub>)<sub>4</sub>(NO<sub>3</sub>)<sub>2</sub>], nickel nitrate hexahydrate [Ni(NO<sub>3</sub>)<sub>2</sub>·6H<sub>2</sub>O], cerium nitrate hexahydrate [Ce(NO<sub>3</sub>)<sub>3</sub>·6H<sub>2</sub>O], citric acid monohydrate [HOC(COOH)(CH<sub>2</sub>COOH)<sub>2</sub> · H<sub>2</sub>O] (CA), polyvinyl pyrrolidone (PVP) were purchased from Sigma Aldrich. All the chemicals were of analytical grade and used as received without further purification for synthesis. Double distilled water was used in the preparation of all the aqueous solutions. Methane, hydrogen, nitrogen, carbon dioxide balanced nitrogen and oxygen gases utilized in this study were purchased from Sigma Gas Services (New Delhi). The purity of all gases was higher than 99%.

#### S1.2 Catalytic characterization:

The crystal structure and phase purity were confirmed by powder X-ray diffraction (XRD) on a Proto Advance X-ray diffractometer fitted with a Lynx eye high-speed strip detector in the  $2\theta$  range  $10\text{-}80^\circ$  using Cu  $K\alpha$  ( $\lambda = 0.154$  nm) as an incident beam.

Surface area analysis was done by Micromeritics ASAP 2020 Surface Area and Porosity Analyser using the BET equation at  $-180^\circ\text{C}$ . Before each experiment, the catalyst was degassed at  $240^\circ\text{C}$  for 3 h under vacuum.

Metal dispersion analysis was carried out in Micromeritics; Auto Chem II 2920 instrument connected with a TCD (thermal conductivity detector). The amount of CO adsorbed was measured by the CO pulse method. The catalyst is first reduced in a flow of  $\text{H}_2$  balance Ar gas at  $500^\circ\text{C}$  for 120 min followed by a purge with He for 45 min, then the catalyst is cooled down to room temperature in an inert atmosphere. After that, a continuous series of 10% CO balance He pulses are injected with an interval of 2 min until the amount of exit CO pulse reaches a steady-state value, it mostly takes 30 pulses.

Thermogravimetric analysis (TGA/DTG) of the samples was carried out by Thermogravimetric analyzer TGA 8000 (Perkin Elmer) instrument using oxygen in the temperature range of  $30\text{-}900^\circ\text{C}$ .

The morphology of samples was recorded on JEM 2100 (JEOL, Japan) transmission electron microscopy, for which all the samples were prepared by dispersing materials in ethanol mounted on a lacey carbon formvar Cu grid. Energy-dispersive X-ray spectroscopy (EDS) was used to perform the elemental analysis using the same spectroscopy. Inductive coupled plasma atomic emission spectroscopic (ICP-AES) was performed using PS 3000 UV, Leeman Labs Inc, (USA) to check the composition of the metals (wt.%) in the catalyst system.

Temperature programmed reduction (TPR) and  $\text{H}_2$  chemisorption experiments were carried out in a Micromeritics, Auto-Chem II 2920 instrument connected with a thermal conductivity detector (TCD). Initially, the 0.05 g sample was first pre-treated under a He stream at 873 K for 120 min and then cooled to room temperature. A 10%  $\text{H}_2/\text{Ar}$  stream (20 ml/min) was passed over the sample while it was being heated from room temperature to 1173 K at a heating rate of 10 K/min.

To find the oxidation state of the catalysts, an X-ray photoelectron spectroscopy (XPS) analysis was performed. X-ray photoelectron spectra were recorded on a Thermo Scientific K-alpha X-ray photoelectron spectrometer, and binding energies ( $\pm 0.2$  eV) were determined with respect to the position of the C 1s peak at 284.6 eV.

The Raman spectra of the catalysts were measured using a laser with a wavelength of 532 nm on a HORIBA Scientific LabRAM HR Evolution Raman spectrometer with an argon laser excitation source. The range of scanned Raman shifts is 50 to 2000  $\text{cm}^{-1}$ .

Inductively Coupled Plasma Atomic Emission Spectroscopic (ICP-AES) analysis was carried out by Inductively Coupled Plasma Atomic Emission Spectrometer; model: PS 3000 UV, (DRE), Leeman Labs, Inc, (USA).

$\text{O}_2$ -TPD was carried out in a Micromeritics, Auto-Chem II 2920 instrument connected with a thermal conductivity detector (TCD) and Mass analyzer (Cirrus 2 mks Spectra Products). Firstly, the sample (100 mg) was heated from room temperature to 600  $^{\circ}\text{C}$  in a He flow of 30  $\text{mL min}^{-1}$ , which was maintained for 100 min, before the sample was cooled to room temperature (He atmosphere), and then the sample was exposed to a stream of 10%  $\text{O}_2$  balanced He (30  $\text{mL min}^{-1}$ ) for 30 min. The sample was then exposed to a He flow for 30 min to clear residual oxygen. After that, it was heated from room temperature to 900  $^{\circ}\text{C}$  in He atmosphere at 10  $^{\circ}\text{C min}^{-1}$ . The  $\text{O}_2$  desorption was continuously analysed using TCD.

The  $\text{CH}_4/\text{CO}_2$ -TPD reaction was performed with a Micromeritics, Auto Chem II 2920 (Micromeritics, GA, USA) instrument connected to a thermal conductivity detector (TCD) and Mass analyzer (Cirrus 2 mks Spectra Products). In order to do this, a 50 mg catalyst was used for the test in a 30  $\text{ml min}^{-1}$  He flow. To prevent any possible impurities, the sample was heated to 600  $^{\circ}\text{C}$  and held for 60 minutes prior to the test. The sample was then cooled to 50  $^{\circ}\text{C}$ , and then the sample was subjected to a 40  $\text{ml min}^{-1}$  10%  $\text{CH}_4/\text{CO}_2$  balance He flows for 90 min to completely saturate the surface, followed by a 30  $\text{ml min}^{-1}$  ultra-high purity He flows for 30 minutes to remove any physically adsorbed  $\text{CH}_4/\text{CO}_2$ . After all of these pre-treatments, the catalyst was heated at a rate of 10  $^{\circ}\text{C min}^{-1}$  from 50 to 900  $^{\circ}\text{C}$  to collect desorption data using TCD. The evolved gas was confirmed with the help of a mass analyzer.

Electron paramagnetic resonance (EPR) spectra were collected at ambient temperature (at room temperature) on a Bruker Biospin, Germany EMX micro A200-9.5/12/S/W to investigate the formation of superoxide species/oxygen vacancy on the catalyst surface. The sample was placed in the capillary tube, and the experimental parameters of EPR were as follows: microwave frequency (9.400 GHz), microwave power (0.715 mW), modulation frequency (100 kHz), modulation amplitude (3.00 G), and sweep time (76.8 s).

### S1.3 Reaction setup and activity measurement

Typically, in a quartz reactor tube having an internal diameter of 6 mm and a length of 34 cm, 60 mg catalyst was diluted with inert material and placed in between two quartz wool plugs in the center of this tube. Before the reaction, the catalyst was reduced at 500 °C for 120 minutes with the flow of 20% H<sub>2</sub> balanced N<sub>2</sub> at the GHSV of 20000 mLg<sup>-1</sup>h<sup>-1</sup>. After reduction, the catalyst was cooled down to reaction temperature and feed gases were introduced into the reactor. Brooks mass flow controllers were used to control the flow rates of the gases. Catalytic performance was investigated in the temperature range of 300-650 °C, where GHSV was varied between 20,000-160,000 mL g<sup>-1</sup> h<sup>-1</sup> with a molar ratio of CH<sub>4</sub>: CO<sub>2</sub>: N<sub>2</sub>=1:1:5. Time-on-stream study of the catalysts was performed at 675 °C temperature where GHSV was 50,000 mLg<sup>-1</sup>h<sup>-1</sup>. The reaction products were analyzed by using an online refinery gas analyzer (Agilent 7890B) fitted with one FID and two TCD detectors. HP-plot-Q column was used for the detection of CH<sub>4</sub> in FID and molecular sieve, hayesep Q, and porapak Q columns were used for the detection of H<sub>2</sub>, CO, and CO<sub>2</sub> in TCD.

### S1.4 DFT Method

Non-periodic, spin-polarized, all electron, numerical basis set-based DMol3 DFT method implemented in Material Studio 8 (Biovia, San Diego, USA) was employed to study the CO<sub>2</sub> and CH<sub>4</sub> activation over the Ni/CeO<sub>2</sub>, Pt/CeO<sub>2</sub> and PtNi/CeO<sub>2</sub> catalysts<sup>1</sup>. Generalized gradient approximation (GGA) Perdew, Burke and Ernzerhof exchange-correlation functional (GGA-PBE) was used<sup>2</sup>. Double numerical plus polarization (DND) basis set with polarized d- and p- functions was employed for all non-hydrogen and hydrogen atoms, respectively.

A transition state (TS) search was performed with the linear synchronous transit/quadratic synchronous transit (LST/QST) method to obtain the transition states for CO<sub>2</sub> and CH<sub>4</sub> activations. During LST, single-point calculations were carried out on linearly interpolated structures on the minimum energy path joining the reactant and product states. The transition state is one which has the maximum energy along this minimum energy path. The structure obtained was taken as an intermediate for QST optimization, resulting in a more refined structure closer to the TS geometry<sup>3</sup>.

Convergence criteria for the DFT calculations were kept at 0.0001 eV, 0.05 eV/Å, and 0.005 Å with respect to energy, force, and atom displacement, respectively.

The activation energy, E<sub>a</sub> was calculated using the following equation,

$$E_a = E_{TS} - E_{IS}$$

Where  $E_{TS}$  and  $E_{IS}$  represent the transition and initial state energies, respectively.

$\text{CeO}_2(111)$  surface slab of  $4 \times 4$  supercell was used having 9 atomic layers, of which the bottom 5 layers were kept fixed to their bulk position, whereas the top four layers were along with the adsorbates were allowed to relax. To model the PtNi/ $\text{CeO}_2$  catalyst, one of the Ce atoms in the top layer were replaced with Ni and one oxygen vacancy was created by removing one oxygen atom for charge balance. One Pt atom was added to the Ni site to obtained PtNi- $\text{CeO}_2$  (111) catalyst surface. Similarly, the Ni- $\text{CeO}_2$  (111) and Pt- $\text{CeO}_2$  (111) surfaces were created. A similar DFT setup has already been used by the authors successfully to study various reactions<sup>4-9</sup>.

## Results and discussion

### Catalyst Characterization:

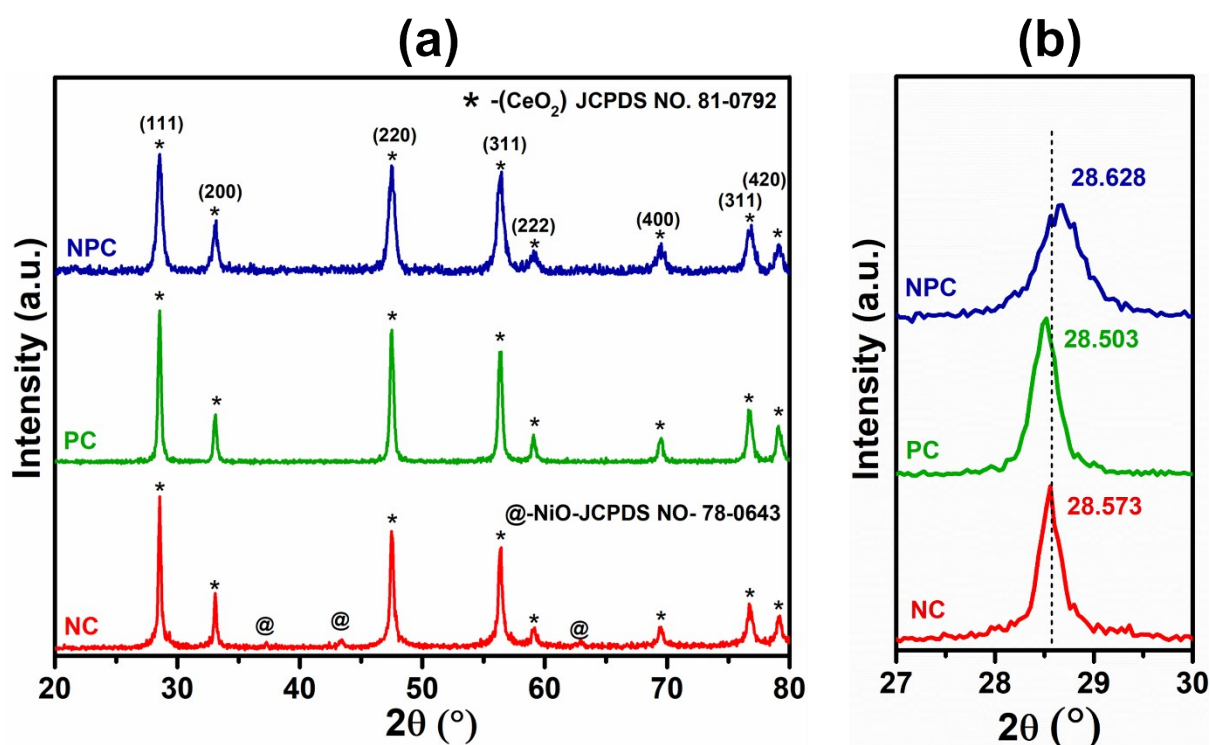


**Fig. S1** Wide angle XRD patterns of spent catalysts (a) and  $2\theta$  shifting with respect to the (111) plane (b). (Reaction condition: Temperature - 675 °C, Pressure -1 atm, TOS - 100 h, and Feed ratio  $\text{CO}_2:\text{CH}_4:\text{N}_2$  - 1:1:5)

**Table S1** Lattice parameter and crystallite size of the catalysts corresponding

to (111) plane of CeO <sub>2</sub>				
Catalyst	Peak position (θ)	FWHM	crystallite size (nm)	Lattice parameter (Å)
CeO <sub>2</sub>	28.476	0.260	31.500	5.4247
NC	28.577	0.785	10.400	5.4056
PC	28.540	0.631	13.000	5.4194
NPC	28.640	1.176	6.970	5.3960

**Table S2** reliability factors of the fit obtained by Rietveld refinement via PROZSKI program

Catalyst	Fit parameters		
	R <sub>Bragg</sub>	R <sub>F</sub>	χ <sup>2</sup>
NC	8.30	5.39	1.25
PC	10.60	5.65	1.30
NPC	8.60	5.60	1.36

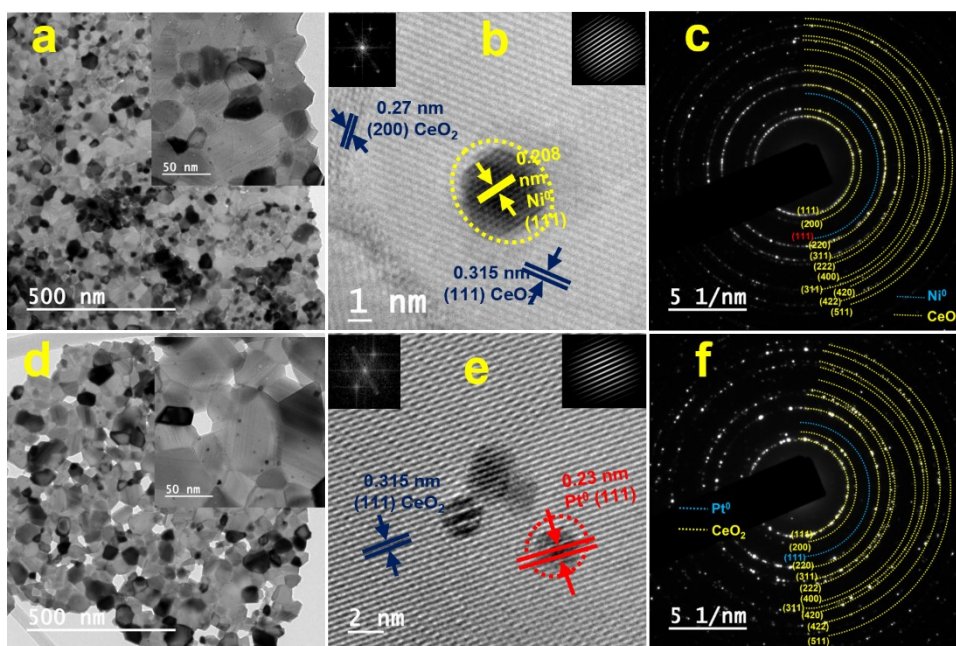


**Fig. S2** TEM/HR-TEM analysis of NC (a, b, c) and PC (d, e, f) catalyst

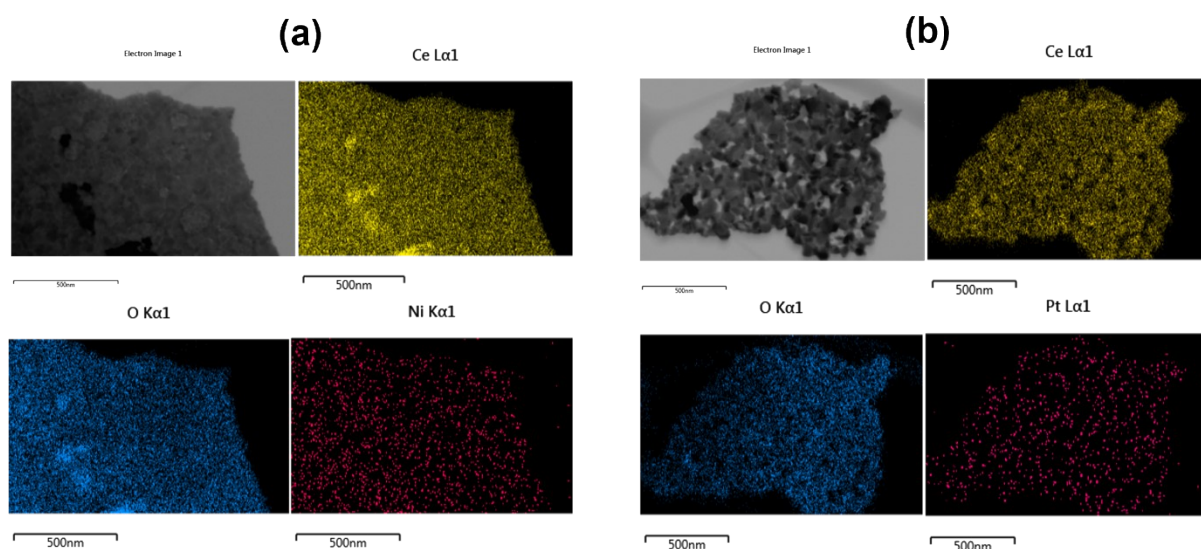


**Fig. S3** Elemental mapping and respective TEM images of NC catalyst (a) and PC catalyst (PC)

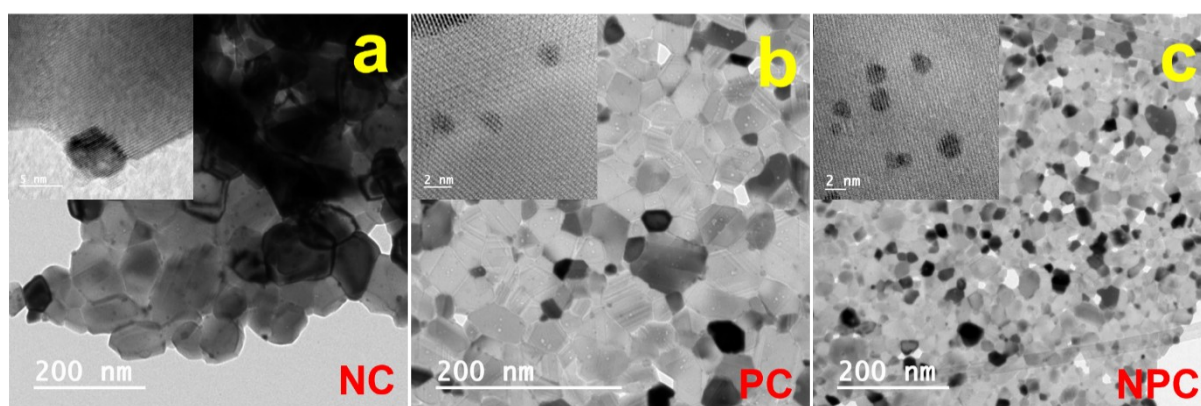


**Fig. S4** TEM analysis of spent NC (a), PC (b) and (c) NPC catalysts after 100 h TOS

**Table S3** BET surface area estimated by N<sub>2</sub>-adsorption isotherm and metal content by ICP- AES

Catalyst	BET Surface area (m <sup>2</sup> /g)		metal content	
	Before rec <sup>n</sup>	After rec <sup>n</sup>	Ni	Pt
CeO <sub>2</sub>	66	-	NA	NA
NC	53	32	1.92	NA
PC	67	64	NA	0.48
NPC	55	51	1.94	0.49

**Table S4** Particle size of metal nanoparticle in nm by HR-TEM images and chemisorption data

Catalyst	average metal particle size by TEM (nm)	average metal particle size by chemisorption data (nm)
PC	2.0	2.1
NC	3.0	3.2
NPC	2.0	2.1

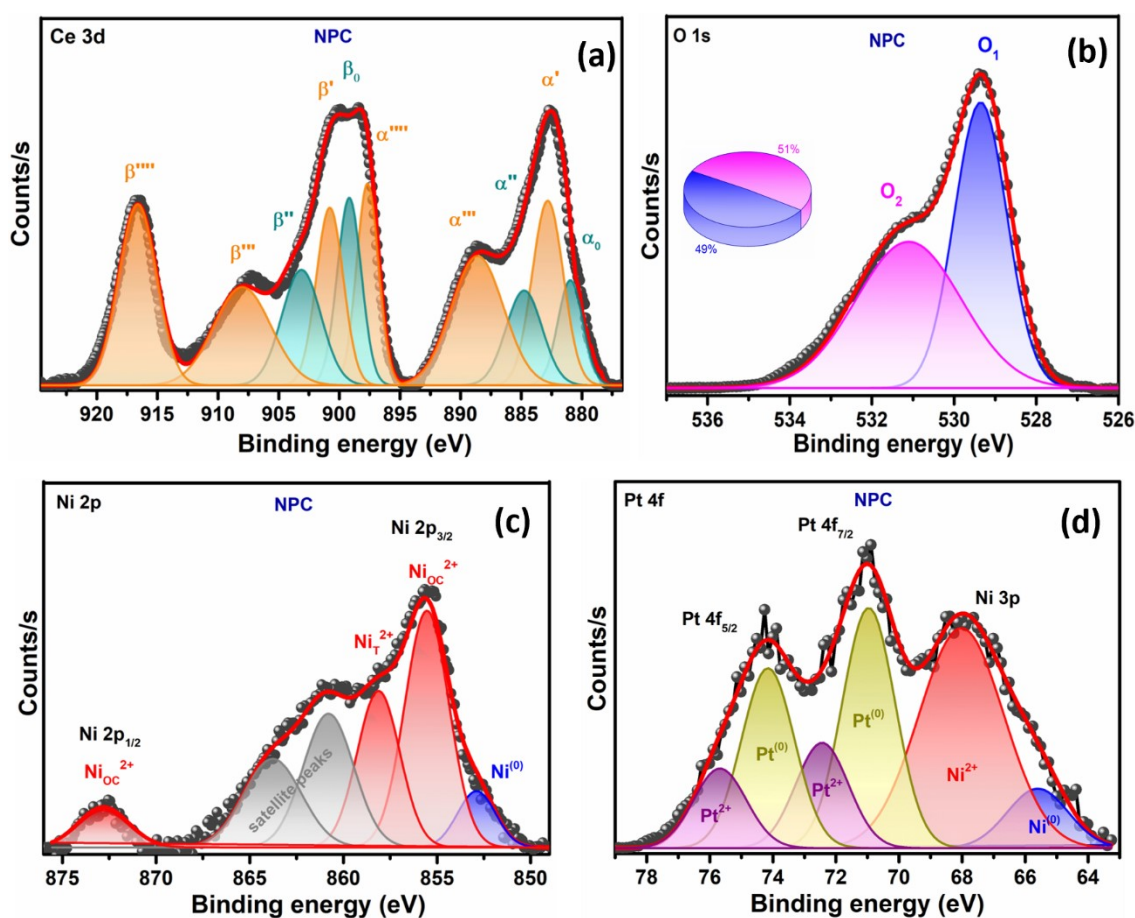


**Fig. S5 (a-d)** XPS spectra of spent NPC catalyst: (a) Ce 3d, (b) O 1s, (c) Ni 2p, and (d) Pt 4f

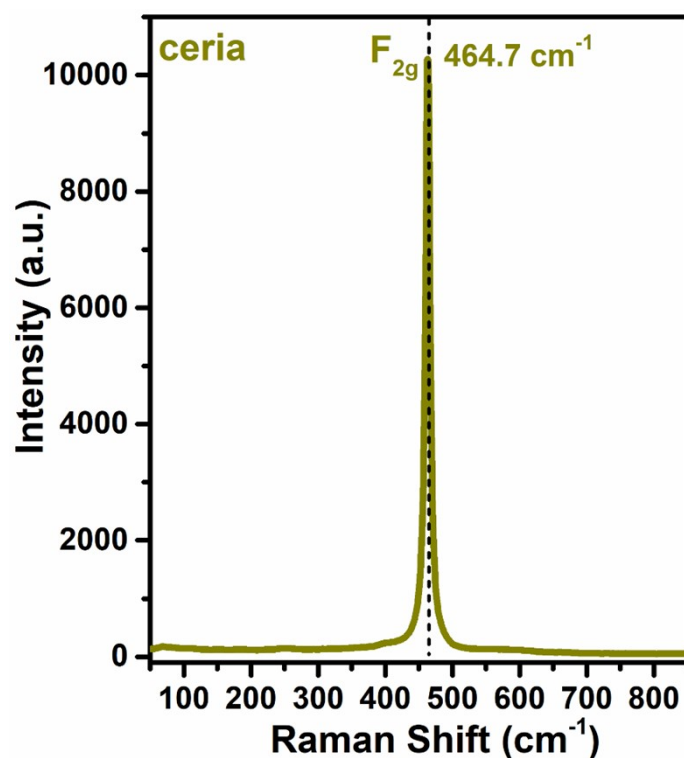


Fig. S6 Raman spectra of commercial ceria

Table S5 distribution of CO<sub>2</sub>/CH<sub>4</sub> adsorption in μmol/g by CH<sub>4</sub>/CO<sub>2</sub> TPD

Catalyst	CH <sub>4</sub> TPD			CO <sub>2</sub> TPD		
	Region I (100-250 °C)	Region II (250-600 °C)	Total (μmol/g)	Region I (100-250 °C)	Region II (250-600 °C)	Total (μmol/g)
NC	16.5	7.6	24.1	5.0	18.7	23.7
PC	20.8	-	20.8	4.0	10.2	14.2
NPC	30.3	13.0	43.3	4.4	27.2	31.6

Table S6 Comparison table for catalytic activities of different catalysts published in the literature

Catalyst	Temperature (°C)	Stability (h)	References
Ru/SiO <sub>2</sub>	800	200	<i>10.1016/j.jcou.2018.12.016</i>
Co(B)/ZrO <sub>2</sub>	750	10	<i>10.1016/j.jcat.2020.09.015</i>

Ni-Mg/ZnO	800	100	<i>10.1016/j.apcatb.2016.03.029</i>
Pt/CePr/Al <sub>2</sub> O <sub>3</sub>	800	24	<i>10.1016/j.ijhydene.2019.09.207</i>
NiMgO	700	24	<i>10.1016/j.apcatb.2020.119056</i>
GdFeO <sub>3</sub>	900	60	<i>10.1134/S0965544120090157</i>
Ni/CeO <sub>2</sub> -Al <sub>2</sub> O <sub>3</sub>	800	72	<i>10.1016/j.apcatb.2020.119459</i>
Ir/Ce <sub>0.9</sub> La <sub>0.1</sub> O <sub>2</sub>	750	200	<i>10.1016/j.cattod.2019.06.067</i>
Pt-Ni@CeO <sub>2</sub>	650	12	<i>10.1039/D1CY00382H</i>
Ni-Mg-Al	800	100	<i>10.1016/j.apcatb.2020.119109</i>
NiO-CeO <sub>2</sub>	800	100	<i>10.1016/j.catcom.2020.105951</i>
Ni-Pt/Ce <sub>0.8</sub> Pr <sub>0.2</sub> O <sub>2-δ</sub>	750	50	<i>10.1016/j.cattod.2019.04.022</i>
Ni-Cu/CeO <sub>2</sub>	800	20	<i>10.1007/s10562-019-02801-y</i>
SiO <sub>2</sub> @Ni@ZrO <sub>2</sub>	700	20	<i>10.1016/j.apcatb.2019.05.021</i>
Rh/γ-Al <sub>2</sub> O <sub>3</sub>	800	180	<i>10.1016/j.fuel.2020.119536</i>
Pt-Ni/CeO <sub>2</sub>	675	100	<b><u><i>This work</i></u></b>

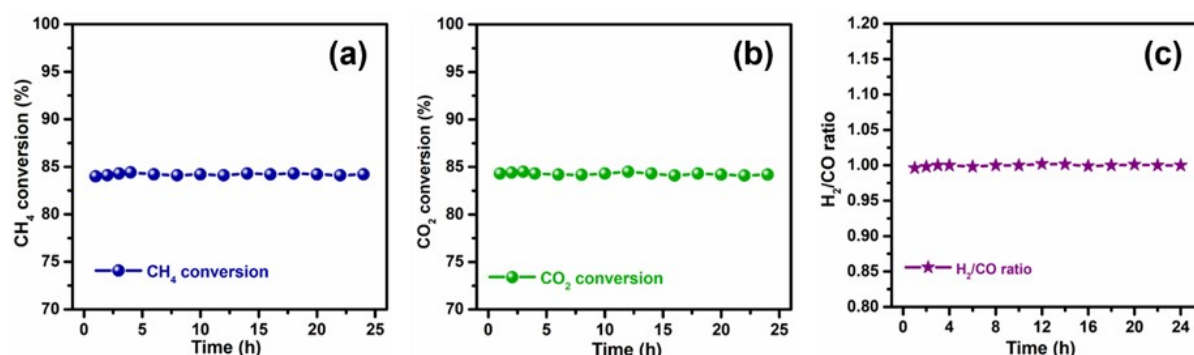


**Fig. S7** Representing the 24 h stability test over the NPC catalysts with undiluted feed at 675 °C temperature and 50,000 mLh<sup>-1</sup>g<sup>-1</sup> GHSV. (a) CH<sub>4</sub> conversion, (b) CO<sub>2</sub> conversion and (c) H<sub>2</sub>/CO ratio

M. Shah et al. reported loss in CH<sub>4</sub> conversion (~ 12 %) when reaction was switched from the diluted feed (CH<sub>4</sub>:CO<sub>2</sub>:Ar - 1:1:8) to undiluted feed (CH<sub>4</sub>:CO<sub>2</sub> - 1:1)<sup>10</sup>. S. Das also reported a decrease in catalytic activity in terms of CH<sub>4</sub> and CO<sub>2</sub> conversion (~ 15%) when reaction switched from the diluted feed (CH<sub>4</sub>:CO<sub>2</sub>:Ar – 1:1:8) to undiluted feed (CH<sub>4</sub>:CO<sub>2</sub> - 1:1)<sup>11</sup>. On the other hand, our catalyst shows almost similar activity throughout the 24 h in the undiluted feed.

#### DFT Results:

CH<sub>4</sub> activation was studied at the Pt nanoparticles supported on the ceria support. The Pt nanoparticle supported on the ceria support was modeled by grafting Pt<sub>6</sub> nanocluster at the CeO<sub>2</sub> (111) surface, as has been shown below in Fig. S8, where multiple Pt-O bonds are formed between the Pt<sub>6</sub> cluster and CeO<sub>2</sub> (111) support.

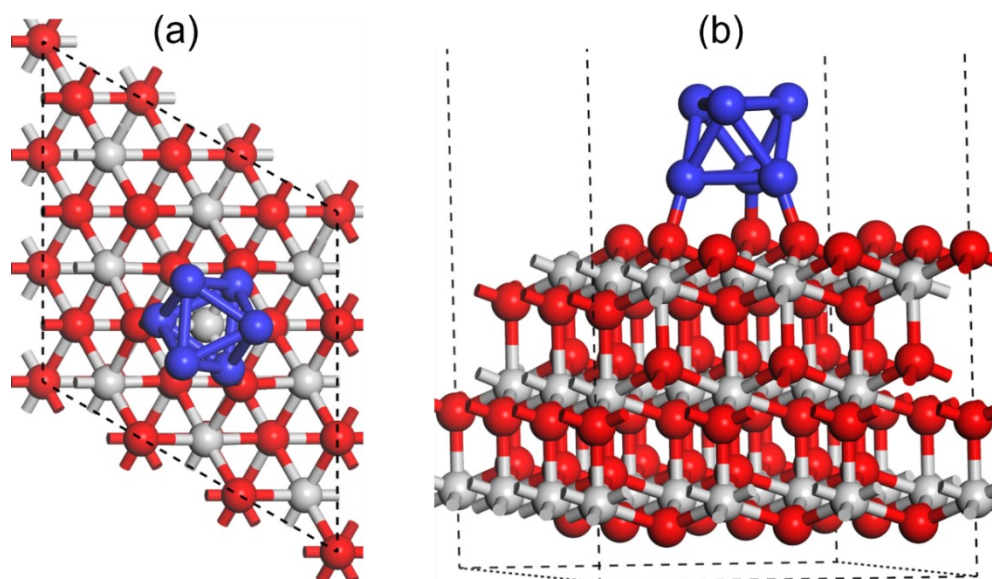


**Fig. S8** DFT optimized geometry of the Pt<sub>6</sub> nanocluster grafted on the CeO<sub>2</sub> (111) surface (a) top view, (b) side view. Color code: Ce (grey), O (red), and Pt (blue)

The geometry of methane adsorbed at the Pt<sub>6</sub> cluster has been shown in Fig. S9. The CH<sub>4</sub> molecule is physisorbed at the Pt<sub>6</sub> cluster with the Pt-C and Pt-H bond distance measured to be 4.3 Å and 3.4 Å, respectively (Fig. S9 (a)). During the C-H bond dissociation at the transition state (Fig. S9 (a')) the C-H bond elongated to 2.3 Å from the initial 1.0 Å in adsorbed methane (Fig. S9 (a)). In the transition state, the Pt-C and Pt-H bond lengths were calculated to be 3.6 Å and 2.7 Å, respectively, as shown in Fig. S9 (a'). The activation barrier for the C-H bond was calculated to be 63.1 kcal/mol. In the final state, as shown in Fig. S9 (b), the C-H bond is completely dissociated forming CH<sub>3</sub> and H, where the Pt-C and Pt-H bond lengths were measured to be 2.2 Å and 1.6 Å, respectively. The reaction energy for the methane C-H bond dissociation was calculated to be endothermic by 17.8 kcal/mol.

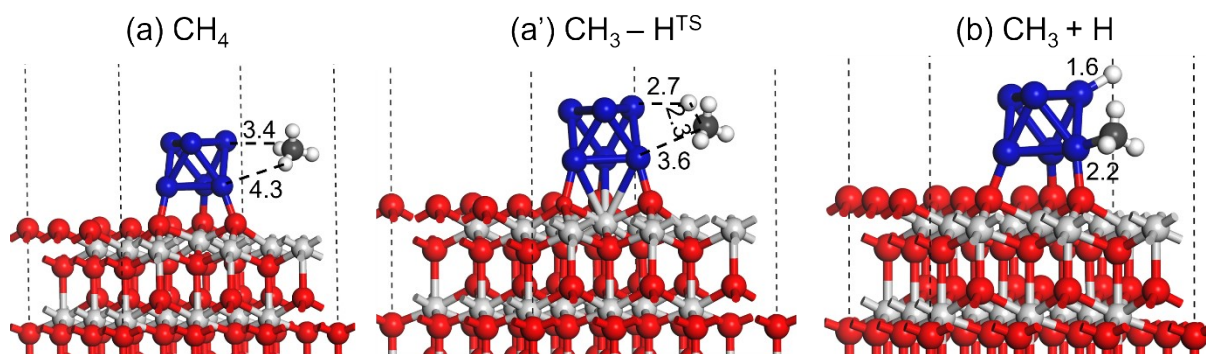


**Fig. S9** Activation of  $\text{CH}_4$  molecule over the (a-b)  $\text{Pt}_6\text{-CeO}_2$  (111) catalyst surface. All bond length values are in Å. Color code: Ce (grey), O (red), Pt (blue), C (black) and H (white)

## References:

1. B. Delley, *The Journal of chemical physics*, 1990, **92**, 508-517.
2. J. P. Perdew, K. Burke and M. Ernzerhof, *Physical review letters*, 1996, **77**, 3865.
3. T. A. Halgren and W. N. Lipscomb, *Chemical Physics Letters*, 1977, **49**, 225-232.
4. R. Khatun, S. Bhandari, M. K. Poddar, C. Samanta, T. S. Khan, D. Khurana and R. Bal, *International Journal of Hydrogen Energy*, 2022, **47**, 38895-38909.
5. S. Bhandari, S. C. Andola, A. C. Kothari, D. Khurana, S. Singh, M. K. Poddar, T. S. Khan, T. Sasaki, V. Prasad and R. Bal, *Journal of Environmental Chemical Engineering*, 2023, **11**, 109380.
6. R. S. Pal, S. Rana, S. K. Sharma, R. Khatun, D. Khurana, T. S. Khan, M. K. Poddar, R. Sharma and R. Bal, *Chemical Engineering Journal*, 2023, 141379.
7. T. S. Khan, S. Gupta, M. I. Alam and M. A. Haider, *RSC advances*, 2016, **6**, 101697-101706.
8. T. S. Khan, S. Balyan, S. Mishra, K. K. Pant and M. A. Haider, *The Journal of Physical Chemistry C*, 2018, **122**, 11754-11764.
9. S. Balyan, M. A. Haider, T. S. Khan and K. Pant, *Catalysis Science & Technology*, 2020, **10**, 3857-3867.
10. M. Shah, S. Das, A. K. Nayak, P. Mondal and A. Bordoloi, *Applied Catalysis A: General*, 2018, **556**, 137-154.
11. S. Das, M. Shah, R. K. Gupta and A. Bordoloi, *Journal of CO2 Utilization*, 2019, **29**, 240-253.